Fusion Engineering and Design 188 (2023) 113426

Contents lists available at ScienceDirect

Fusion Engineering and Design

journal homepage: www.elsevier.com/locate/fusengdes

Creep fatigue analysis of DEMO divertor components following the RCC-MRx design code

M. Muscat [a,*], P. Mollicone [a], J.H. You [b], N. Mantel [c], M. Jetter [d]

[a] Department of Mechanical Engineering, Faculty of Engineering, University of Malta (UM), Malta
[b] Max Planck Institute for Plasma Physics (IPP), Garching, Germany
[c] Culham Centre for Fusion Energy (CCFE), Abingdon, United Kingdom
[d] Karlsruhe Institute of Technology (KIT), Karlsruhe, Germany

ARTICLE INFO

Keywords:
Design by elastic analysis
Type-P damage
Type-S damage
High temperature
Creep-fatigue
RCC-MRx
DEMO divertor

ABSTRACT

In the DEMO fusion reactor, in-vessel components will be subjected to very high thermo mechanical steady and cyclic loads. A design check that is required by the RCC-MRx code used for nuclear installations and fusion reactors is a creep-fatigue check. The fatigue damage is caused by the pulsed operation of the fusion reactor while creep damage occurs during the hold time of loads at elevated temperatures. The temperature of the main divertor components is kept below that which causes creep by using cooling fluid that flows through channels fabricated within the components themselves. Other components such as the shielding liner and reflector plate supports on the divertor cassette cannot be cooled as such and so their temperature can rise high enough so that they sustain creep damage. In the presence of creep, the fatigue life of a component is reduced. In this work, a creep fatigue assessment of a representative simple geometry is carried out. The representative geometry is that of a thick cylinder under the action of steady and fluctuating loads similar to those seen by DEMO in-vessel components while in service. The cylinder example creep fatigue results are used as a benchmark and compared with those obtained using the creep fatigue assessment (CFA) tool developed at KIT (Karlsruhe Institute of Technology). Methodologies used for creep fatigue assessments within RCC-MRx are presented and explained and results discussed. The work should provide a contribution towards any necessary creep fatigue assessments of DEMO divertor components currently being developed.

1. Introduction

The European DEMOnstration Fusion Power Plant (DEMO) pre-concept design stage was brought to an end and finalised in 2020. A number of work packages concentrated on the different reactor components. One of these work packages was dedicated to the divertor of the reactor [1]. The divertor is one of the main in vessel components having Plasma Facing Components (PFCs). The plasma is contained in a nominal D-shaped cross section shaped torus by the strong magnetic fields created by the toroidal and poloidal magnets which lie outside the tokamak vacuum vessel. The malfunction of a magnet, a failure of the control system and the presence of impurities can trigger a plasma disruption so that the latter moves away from its confined designed position. In a fusion power plant such disruptions can severely damage parts of the reactor especially the first wall and divertor. The damage is mainly caused by the high temperatures seen by the components and the large currents going through them. Damage can be reduced by having a control system that can predict a disruption and that attempts to stop the plasma current and dissipate the plasma's heat energy by spreading it over the whole first wall and the whole set of divertors. Apart from handling disruption events which, in a fusion power plant, must be avoided as much as possible, one of the main functions of the DEMO divertor is to deal with the constant loss of particles and energy from the plasma. Particles can move very fast along the magnetic field lines but turbulence causes the particles to move outwards towards the open magnetic field lines. In DEMO the edge of the plasma is defined by using a magnetic X-point. The X-point is a magnetic surface that intersects or crosses itself and is created and positioned by the poloidal field coils. The X-point distinguishes the end of the closed and the start of the open magnetic field surfaces. The closed magnetic fields confine the plasma while the open ones do not. The X-point is positioned just above the divertor so that when turbulence causes plasma particles to migrate

* Corresponding author.
E-mail address: martin.muscat@um.edu.mt (M. Muscat).

https://doi.org/10.1016/j.fusengdes.2023.113426
Received 30 September 2022; Received in revised form 14 December 2022; Accepted 16 December 2022
Available online 11 January 2023

outside the closed magnetic field lines they hit the target plates where they deposit their energy. This energy is removed as thermal energy by cooling fluid passing through the copper alloy cooling pipe surrounded by the tungsten monoblock armor of the target plates [1]. Another main function of the divertor is to guide the particles of exhaust helium 'ash' and unburnt fuel (deuterium-tritium) towards the pumping ports below the shielding liner. Helium 'ash' needs to be removed out of the plasma to keep its concentration below the dilution threshold so that the plasma remains stable. The plasma core continuously radiates fast neutrons that generates volumetric nuclear heating in the divertor components. Irradiation would be the cause of embrittlement of the materials of the divertor components so this needs to be taken into consideration in any structural integrity assessment. Ref. [1] gives more details on the loads and different load cases acting on the divertor. Refs. [1–6] give further detailed descriptions of the development of the pre-conceptual design of the divertor cassette body, cooling systems, target plates, reflector plates, shielding liner and cassette support system within the vacuum vessel. The latter development takes into consideration manufacturing, fabrication and assembly processes and related heat transfer and preliminary structural integrity issues. Refs. [1,5,6] give details of load specifications and of the different load cases and critical design issues that are still under study.

In [7] You et al. give more detail on the structural design of the divertor vertical targets. These are subjected to relatively extreme and complex loading conditions such as high heat fluxes, intense particle bombardment, fast neutron irradiation, fluctuating stresses and impact loads. Similar extreme conditions exist for the other divertor components. Currently there are gaps in the existing knowledge on how the different loads on the divertor targets and other components interact together and how the latter affect the material properties and structural integrity of the same components. Different failure modes must be taken into consideration and the authors in [7] stress on the importance of using both a Design by Experiment, a Design by Analysis (DBA) and a Design by Code approach. At the moment, a full Design by Experiment approach is not possible because currently there is no existing nuclear testing facility. This therefore requires extensive recourse to DBA and Design by Code approach which make use of the latest developments on material properties and design improvements. The DBA approach for the design of divertor components is sometimes not fully applicable as relevant design codes are still under development. DBA can therefore complement the Design by experiment and design by code approach but is quite valid especially in the initial iteration of the design process and as further improved material properties and load specifications become available. Another issue highlighted in [7] is that of initial residual stresses brought about by fabrication and welding processes. From a structural integrity point of view residual stresses are important when considering the failure modes involving creep and fatigue. Calculating the residual stresses in any component is not a trivial task and may involve using a complex visco-plastic constitutive model when simulating the fabrication or welding process. Other material property issues that were considered in [7] deal with softening due to thermal aging and embrittlement brought about by high thermal stress and low temperatures.

The computer aided design (CAD) model for one of the divertor cassette module developed during the pre- conceptual design phase is shown in Fig. 1. The adopted baseline model is called the 'single null' divertor in which the latter is located at the bottom of the vacuum vessel. This baseline model has a dual cooling circuit system.

Ref. [8] describes the preliminary development of a thermal and structural finite element (FE) model for one of the DEMO divertor cassette modules. Initially, the main loads i.e. the electromagnetic loads including disruption events, the pressure loads due to the water inside the cooling channels, convective loads and thermal neutron loads were considered. Estimates of such load values were obtained from the ITER design. The design methodology followed the elastic DBA rules of the French code 'Design and Construction Rules for Mechanical Components

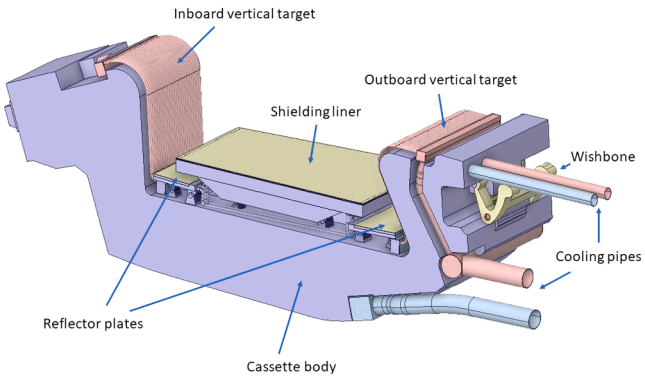

Fig. 1. One of the DEMO cassette modules including shielding liner, reflector plates, vertical targets and inlet and outlet cooling pipes.

of Nuclear Installation (RCC-MRx)' [9]. The EUROFER97 material was adopted for the divertor cassette and main sub components while a tungsten layer was used on the surfaces of the shielding liner and reflector plates. The latter's material properties were obtained from [9]. Ref. [8] includes a preliminary elastic-plastic analysis based on the isotropic hardening rule utilising temperature dependant material properties. Kinematic boundary conditions were such as to allow radial expansion of the cassette under thermal load. As a preliminary evaluation using elastic analysis and following RCC-MRx [9] creep effects were considered negligible [8]. Because of lack of data for EUROFER97 steel the analysis was carried out for unirradiated conditions. In [8] Frosi et al. conclude that thermal loads have a huge influence on the structural assessment of the divertor cassette and attention must be given to the supports fixing the divertor cassette to the vacuum vessel in order to reduce stresses and strains in those regions.

In [10] Frosi et al. improved on the FE DEMO divertor cassette model. Such improvements included optimisation of the FE mesh, a better estimate for the volumetric nuclear power density and convective cooling loads in the cooling channels and the inclusion of the contribution of halo currents to the resulting electromagnetic forces and moments. In [10] load values from neutron and electromagnetic computational analyses carried out for the DEMO cassette (rather than ITER derived loads) were used. As an assumption, the nuclear heating load and the electromagnetic loads were applied uniformly over the cassette body. In reality, for the nuclear heating loads, higher values are found in the inboard regions rather than in the outboard regions. The thermal analysis gave the temperature distribution for the different load cases for the mechanical and thermal structural analysis. Similar conclusions as in [8] about the relative importance of the thermal loads when compared to the water cooling pressure in the divertor channels were made. Higher stress values than in [8] for load cases involving the electromagnetic loads were found. Ref. [10] also dealt with creating a shell model for the cassette. This was used to optimise its internal rib layout and thicknesses. These ribs make up the internal construction of the divertor cassette and effectively form the layout of the water cooling channels. The external shell thickness of the cassette was also optimised.

In [11] Frosi et. al. improved once again on the divertor cassette FE structural model. The main improvements on previous work was that the thermal and electromagnetic loads were now applied according to the proper distribution obtained from neutron and electromagnetic analyses. It was again concluded that for all load cases the values of stress are dominated by the thermal and electromagnetic loads rather than by the cooling water pressure. Furthermore, the latest design for the inboard and outboard cassette fixing supports did not meet the RCC-MRx elastic stress allowables. Further analysis [1,12–14] led to the eventual development of the cassette supports for the dual circuit baseline model shown in Fig. 1. The final so called wishbone design of the outboard support introduces a preload in the cassette body both

during stand by conditions and also at full load conditions. The preload keeps the cassette in the correct position relative to the vacuum vessel. Refs. [12–14] also describe the development carried out on the shielding liner and on the reflector plates. The former is used for shielding the cassette and vacuum vessel from radiation and neutron flux. The latter is used for the protection of the plasma facing components' cooling manifolds and diffusers from irradiation. The uniform surface heat load impinging on the shielding liner and reflector plates is as yet unknown and an estimate has been used for performing the thermal structural analysis.

The pre-conceptual design of the DEMO divertor cassette module has reached a level of maturity where a number of key findings and remaining open issues were identified [1]. Ref. [1] lists a number of points to be considered in the conceptual design phase (2021 – 2027). The list touches on issues related to an alternative design concept for easier remote handling, to rigorous structural integrity assessments for steel irradiated below the ductile to brittle transition temperature, to design for manufacturing and the effects on structural integrity issues and to experimental design approaches for high heat flux verification of components.

2. Design and stress analysis methodologies and RCC-MRx

The current major structural integrity design codes normally use three approaches for design. These are Design by code rules (DBR), Design by experiment (DBE) and Design by Analysis (DBA). DBR is used for standard components, loadings and boundary conditions. The DBR route guarantees a safe and reliable design. These rules have been improved and validated so that they include years of experience on the life time integrity of a particular component. DBE is very useful for validation purposes of mock ups but in certain cases might not be possible because of lack of facilities or because of manufacturing difficulties. DBA is used for those cases not covered by DBR and where DBE is not yet possible for various reasons. DBA allows the designer or analyst to use any applicable computational methodology to evaluate the stress and strain fields in the component for the case of a structural stress analysis. Most stress analysis design codes contain an elastic approach and an elastic plastic route. The elastic plastic route, sometimes also called the direct route, addresses failure modes directly and should result in safe but less conservative designs. Having said that, the elastic route seems to be as yet the most common amongst analysts. This may be due to a number of reasons maybe the most common ones being lack of material data to perform elastic plastic analyses, lack of computational hardware facilities that can handle elastic plastic analyses and large models and also due to the confidence that has been built in the elastic design approach over the years in the pressure vessel and nuclear power industries.

The literature review given in the introductory section shows that the most common approach used for the stress analyses of the pre-conceptual design of the DEMO divertor has been the elastic route. Having said that, the elastic plastic route has been used in monotonic type of loading analyses to get an overall view of the stress and strain fields and indicate where plasticity would be expected [10–12,14].

The French nuclear code RCC-MRx [9] has been used extensively for the pre-conceptual design phase, this being mainly due to the code's maturity in the nuclear power plant field. The latest edition of RCC-MRx is the 2018 edition [15]. RCC-MRx can be used within the scope of sodium-cooled fast reactors, research reactors and fusion reactors. It is made up of a number of volumes dealing with material testing requirements, material properties for a relevant range of materials including EUROFER97 (still under development and in the probationary phase), weld material properties, welding processes, component fabrication processes, examination methods and design methodologies. The latter are found in Section III, Tome 1, Volume B, RB3000. RB3000 covers 'General Design Rules', 'Design by Analysis' and Design rules for specific components such as shells, vessels, piping, box structures and heat exchangers amongst others.

The design rules aim to prevent failure due to immediate excessive deformation, immediate plastic instability, time dependent excessive deformation, time dependent plastic instability, time dependent fracture and fast fracture, elastic or elastoplastic instability (buckling), progressive deformation and fatigue. The first six failure modes are brought about by type P damages which arise from steadily and monotonically increasing loads or constant loads. The last two failure modes are brought about by type S damages which arise from cyclic loads. Creep at elevated temperatures accelerates the damage due to fatigue and so can become a critical failure mode if the operating temperature is above the negligible creep temperature for the material.

Design is affected by the component's operating conditions. These are classified under four categories. The 1st and 2nd category of operating conditions include normal operation and normal operating incidents, start up and shutdown. The 3rd category includes emergency conditions having very low probability of occurrence but which would require plant shut down and the necessary inspection. The 4th category of operating conditions are highly improbable but are considered because of safety reasons. Each operating condition is characterised by a set of loads. In RCC MRx load cases are referred to as loadings and are a set of loads corresponding to each operating condition. RCC MRx defines three levels of criteria (A, C and D) to be met by the component for each set of loadings associated with an operating condition. Level A criteria is the highest level and prevents failure against all the above mentioned failure modes for the life time of the component. The level C criterion excludes fatigue and creep fatigue type of failures so that analysis using this criterion limits the component to 10 cycles of loading. Level D criterion prevents the failure modes as for the level C criterion but with a lower margin of safety. RCC MRx requires that components designed on the 1st and 2nd category meet the level A criteria, those designed on the 3rd category need to meet the level C criteria while those designed on the 4th category need to meet the level D criteria.

RCC MRx requires a corrosion, erosion and wear allowance if such conditions occur during in service conditions. For type P damage the corroded thickness must be used for design while for type S damage the nominal non corroded thickness can be used. RCC MRx also requires the analyst to, if necessary, include the effect of thermal aging and irradiation on the material properties.

The stress analysis of DEMO divertor components must initially consider 1st and 2nd category of operating conditions which include normal operation and normal operating incidents, start up and shutdown [14]. The 3rd and 4th category of operating conditions can be considered once the divertor design reaches the necessary level of maturity. 1st and 2nd category of operating conditions require RCC MRx code assessment at level A criteria, which requires the analyst to perform all the required type P and type S damage checks. Previous work has already included some type P and type S damage checks and analyses [8,10,11,13,14] but creep type P damage checks and fatigue and creep fatigue assessments which fall under type S damage checks have as yet not been carried out.

3. Fatigue and Creep-Fatigue assessments following RCC-MRx

Ref. [16] gives a summary of type P and some type S damage checks carried out on the DEMO divertor shielding liner components and their supports under the action of thermal, electromagnetic and cooling water pressure loads inside the cooling channels. The checks followed the RCC-MRx elastic analyses route. Separate analyses were performed for each different type of load under non irradiated and irradiated conditions. Some EUROFER97 material properties were not available and substitute material data was used. This may have affected the results but was deemed to be a good first attempt at a number of structural integrity assessments. Progressive deformation was assessed using the $3S_m$ rule but fatigue and creep fatigue assessments were not carried out. The authors in [16] report high temperatures in the shielding liner supports

(lugs, pins and connecting rod) causing these components not to meet the RCC-MRx 'Level A' code criteria for type P damage and for the $3S_m$ type S damage check for ratchetting. These supports are shown in Fig. 2.

The reason for the high temperatures in these regions is due to lack of cooling in the supports. Material allowable stresses are lower at elevated temperatures. This may in the future require changes in the support dimensions or even a complete re-design of the supports themselves. Some temperatures, especially in the supports and for certain loadings, were reported to be above the creep temperature for EUROFER97 steel. For EUROFER97 the temperature above which creep becomes significant is 375°C whatever the holding time [15]. Such regions i.e. the shielding liner and reflector plate supports, would require creep rupture and excessive creep strain analysis for type P checks and creep fatigue assessment for type S checks, especially when cyclic loadings are applied.

RCC-MRx [15] gives the required type P damage and type S damage checks when creep is significant for both negligible irradiation and also when irradiation is significant. The type S damage checks include progressive deformation analyses, fatigue and creep fatigue analysis. Lejeail et.al. [17] conclude that design rules for nuclear steel components such as RCC-MRx [15] can be very complex. These become much more so at elevated temperatures when creep becomes significant and when cyclic hardening or softening affects the creep behaviour. Such effects are considered both in the elastic and elastic plastic approaches to design. The rules for the elastic approach tend to be more complicated since these need to include calculations that mimic plastic material behaviour [15,18–21].

In the presence of creep, the type P damage checks are simpler to apply than the type S damage checks so that this paper concentrates mostly on the latter. Having said that, as a prerequisite, the creep fatigue analysis requires the type P and progressive deformation type S check to be acceptable to the code [15]. Literature review and the code itself [15] reveals that the RCC-MRx elastic route for creep fatigue assessment requires a multitude of calculations for each stress classification line (SCL) selected for analyses. The SCLs are used in the elastic analysis approach in order to characterise the membrane, bending and peak stresses. These can then be categorised into primary and secondary stresses. Primary stresses (such as membrane stresses that are uniform across the wall cross section and bending stresses that are required to keep the component in equilibrium with the external loadings) have different allowables to secondary stresses (such as thermal stresses and bending stresses at gross structural discontinuities). A number of SCLs are normally required to assess a component and so such an assessment can become laborious and highly prone to error. This has compelled researchers to develop computational tools that can be used by the stress analyst to perform such an assessment [22,23]. These tools are always under development and features are added to them according to the component application and loadings. It is also good to remember that the SCL technique is more appropriate for thin shells.

The creep-fatigue assessment (CFA) tool of particular interest to the work in this paper is the one developed at the Karsluhe Institute of Technology (KIT) [23,24–27]. In [23] Özkan and Aktaa presented the initial development of the KIT CFA tool which utilised the ANSYS MAPDL software and FORTRAN coding to analyse fusion reactor in-vessel components operating at high temperatures and cyclic loading. The tool was based on the ASME Boiler and Pressure Vessel Code creep fatigue elastic route rules [28] adapted for EUROFER97 steel [24] to perform a preliminary analysis on a Helium Cooled Pebble Bed Test Blanket Module (HCPB-TBM) for the First Wall component of the TBM box for the DEMO fusion reactor. The CFA tool could analyse the component at different irradiation conditions and for different holding times. At the time, the CFA tool required the analysts to define the paths in critical regions along which the assessment was going to be carried out, the irradiation rate and the load holding time.

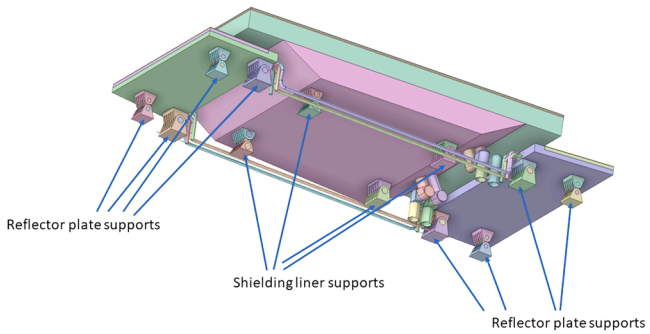

Fig. 2. Shielding liner and inboard and outboard reflector plate supports.

In [25] Mahler et al. extended the KIT CFA tool to automatically identify the most critical path. This requires a definition of a region of interest in ANSYS Mechanical or Mechanical APDL. One region must be on the inner and one on the outer surface of the component under evaluation. Once the analyst identifies the inner and outer surfaces to define the region of interest, the CFA tool determines the number of nodes lying on these surfaces. Starting with the surface that contains the smallest number of nodes it searches for the minimum distance between the inner and outer region and selects all elements which are on the paths of minimum distance. Mahler et al. argue that using only the paths of minimum distance is an acceptable assumption since this strategy follows the code rules for selecting paths for stress linearization. The CFA tool then linearizes the stresses along all the identified paths and determines the fatigue life and the creep and fatigue damage by calculating the elastic strain range for the thermal, primary and primary plus secondary loadings. After calculating the fatigue life (allowable number of cycles) and minimum time to rupture for each possible path, the CFA tool identifies the most critical one. Based on the latter, the fatigue and creep damage for this path together with the fatigue life are evaluated.

In [26] Mahler and Aktaa describe the further improvements made to the KIT CFA assessment tool. The tool is self-contained and can be used within the ANSYS Workbench environment utilising the software applications ANSYS Mechanical, ANSYS MAPDL and FORTRAN coding. It requires the user to input the FE model including boundary conditions and load actions, to specify whether to use elastic analyses or inelastic analyses, to specify the region of interest (ROI) where to perform the creep fatigue assessment within the model and other data such as material properties and the code of standard to use (ASME or RCC-MRx) for the assessment. The tool has the built-in specific material (EUROFER97) design fatigue curves, the creep stress versus time to rupture curves, the monotonic and isochronous stress versus strain curves the latter three all at different temperatures and the creep-fatigue damage interaction diagram. For the elastic analysis route the tool uses the FE calculated local stress, maximum elastic strain range and temperature. Coupled with stress linearization the tool calculates a modified equivalent strain range that takes into consideration inelastic effects. In addition, Aktaa implemented a modified rule [27] to improve the underestimation of creep damage caused by the cyclic softening behaviour of EUROFER97 steel. In this modification the required stress is multiplied by a factor called K_Ψ which considers the effect of cyclic softening on stress to rupture curves. The inelastic analysis route can be used if the elastic route is too conservative. For the CFA elastic route three simulations are required. These are

(1) a thermal analysis to obtain the steady state temperature stress field
(2) a structural analysis which considers only the primary loads. These are essentially applied load actions that cause primary stresses
(3) a structural analysis which considers the primary and secondary loads at the same time. Secondary loads would normally be the temperature loads

Over the years other improvements made to the KIT CFA tool included replacing the predicted isochronous stress v.s. strain curves with curves obtained experimentally and changing the structure of the CFA tool to accept other material data other than EUROFER97. In 2018 the Creep-Fatigue assessment procedure based on the RCC-MRx code [9] was implemented in the KIT CFA tool so that the elastic as well as the inelastic RCC-MRx Creep-Fatigue rule is available in the current version of the CFA tool [29]. In 2020 Jetter M. updated a guide for using the KIT CFA tool and carried out a comparison between the manual calculations for creep fatigue assessment following the RCC- MRx rules for elastic analyses of a CEA Breeding Blanket model with the results from the KIT CFA tool [30]. Further work was carried out on the results from [30] to identify the reason for any diverging result values. In 2021 the creep stress relaxation during the hold time for secondary stress allowed for in the elastic route presented in RCC-MRx was integrated in the CFA tool [31,32]. This latest improvement would make the component design more efficient in terms of material usage but still ensure that the component remains fit for purpose for its predicted lifetime.

4. The thick cylinder benchmark model

In view of future creep fatigue assessment of DEMO divertor components, the WPDIV group within the EUROfusion consortium embarked on the task of making use of the latest version of the KIT CFA tool [30]. The use of the KIT tool for creep fatigue assessment would be contributing to reducing the time necessary for the DEMO divertor design cycle. Use of the KIT CFA tool requires familiarity with the tool application and is an opportunity to suggest improvements on the tools' capabilities to further develop it for the DEMO divertor components' load cycles and geometries. This section deals with a creep fatigue assessment (using the elastic approach) of a thick cylinder under the action of steady and fluctuating loads similar to those seen by DEMO in-vessel components. The example is used as a benchmark application for the KIT CFA tool. Manual calculations following the RCC-MRx creep fatigue rules [15] for the thick cylinder are carried out and results compared with those obtained using the CFA tool developed by KIT. A summary of some calculations used for elastic creep fatigue assessments within RCC-MRx [15] for the thick cylinder model are presented and explained and result divergence and code implementation issues discussed. The axisymmetric thick cylinder benchmark model used for the exercise is shown in Fig. 3.

The thick cylinder model has a finite length of 1000mm with free ends. It is subjected to an internal pressure of 8MPa while the outside pressure is zero. The internal and external wall temperatures are 500°C and 350°C respectively. Both pressure and temperature loads are cycled together so that they cycle proportionally between a value of zero and their maximum values at any point in the model. The hold time for both pressure and temperature loads is 1 h. The material properties are those for EUROFER [15]. For the coefficient of linear thermal expansion the average temperature properties are used. The reference temperature for the coefficient of linear thermal expansion material property is set to 20°C. The environment temperature is also set to 20°C indicating that the model has zero residual stresses at this temperature. A finite element model was developed in ANSYS Mechanical [33]. Fig. 4 shows the temperature distribution, FE mesh and equivalent stress plots across the model for both the primary and primary plus secondary stresses. The primary von Mises stress intensity was obtained by applying the internal pressure and taking into account the material property variations due to the temperature gradient. The primary plus secondary stresses were obtained by also including the thermal stresses.

5. Creep-Fatigue assessment - KIT CFA tool

Fig. 5 shows a summary of the results from the KIT CFA tool for the thick cylinder model. For the given loads described in Section 4 of this paper the tool predicts that the number of cycles to failure is 119671. At

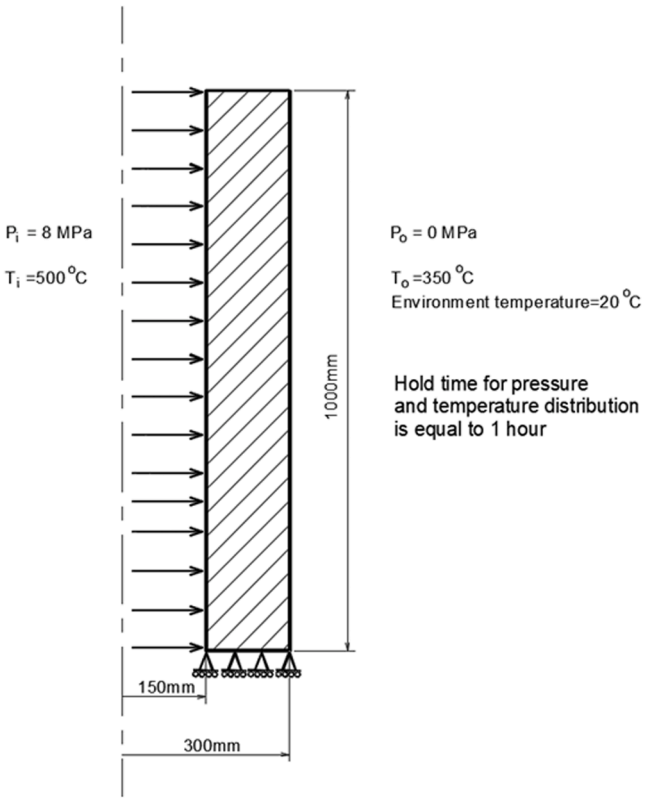

Fig. 3. Thick cylinder benchmark model.

failure, creep damage would be 74% while fatigue damage would be 11%. These percentages are given with respect to 100% creep or fatigue damage if the failure modes are considered as not interacting together to cause failure. Fig. 5 also indicates the critical SCL at which initial failure is predicted to occur. Table 1 gives various other input parameters and output results required for the creep fatigue assessment and obtained as output from the KIT CFA tool respectively. In the same table these parameters are compared with the manual calculated ones and any discrepancies are highlighted and discussed later on. For this paper the manual calculation is only performed for the critical SCL as identified by the KIT CFA tool. Manually, for the considered thick cylinder model, the critical path is laborious to locate and a number of paths need to be considered for this purpose. This is one advantage of using an automatic tool for the analyses. When performing a manual analysis it is usual practice for the analyst to consider critical regions such as stress concentration points, regions of high temperatures and any other region that may be known to suffer failure of any kind.

6. Creep-Fatigue assessment - manual calculations

In RCC-MRx the type S damage checks only apply if the type P damage checks are satisfied [15]. Therefore, to conduct a creep fatigue assessment all the DBA type P and type S analyses need to be carried out for all the SCLs that are considered. For the thick cylinder benchmark model buckling failure is not anticipated so that this type of analyses is not carried out. Furthermore, the model does not have any welded regions so that material properties are for parent EUROFER97 steel with no adjustment for welding. To start with, RCC-MRx requires the analyst to conduct negligible creep tests and negligible irradiation tests. These affect the DBA design rules to follow. Given the lack of availability of irradiation material property data for EUROFER97 steel, the analysis explained below considers only non-irradiated components. Level A assessment criteria for the 1st category of loading is considered.

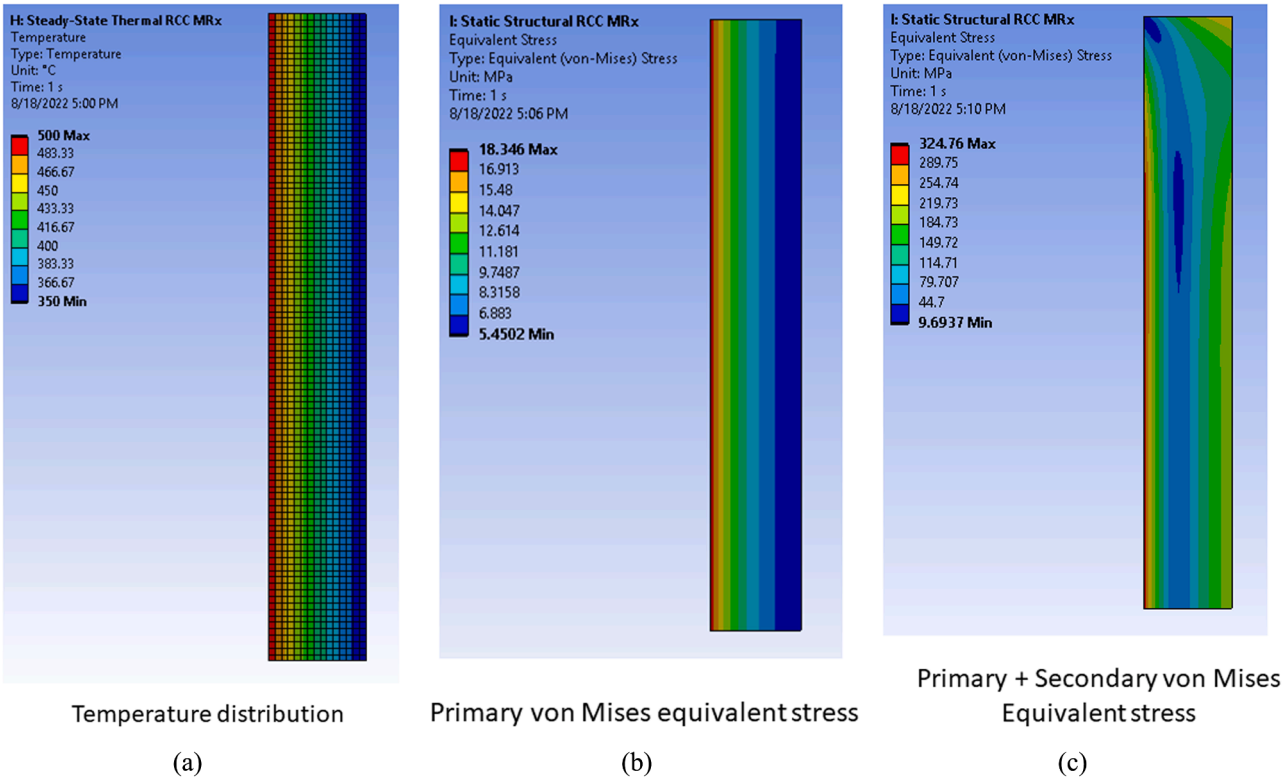

Fig. 4. (a) Temperature distribution and FE mesh, (b) Primary von Mises Equivalent stress, (c) Primary + Secondary von Mises Equivalent stress.

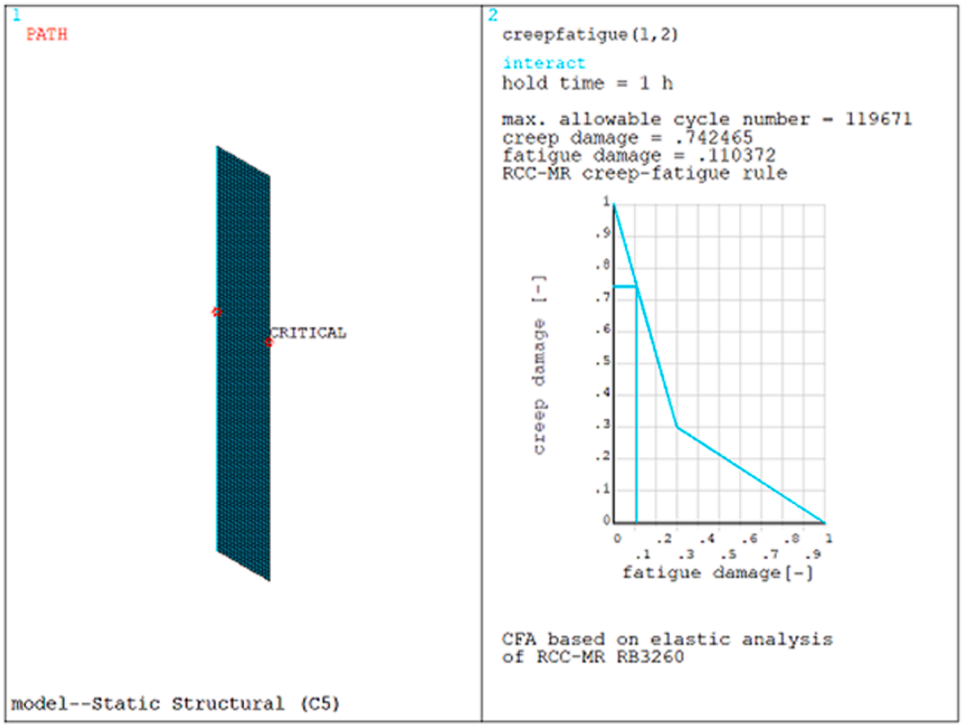

Fig. 5. KIT CFA tool basic results for the thick cylinder model.

6.1. *Negligible creep tests*

In RB 3216.1 RCC MRx presents two tests for deciding whether creep is to be included in the analysis. In the first part of the first test, which is the only test applicable for this example, the maximum operating temperature is compared with the material creep threshold temperature. For EUROFER material in A3.31, creep is not negligible for temperatures higher than 375°C for any holding time [15]. The outer wall temperature for the thick cylinder is 350°C i.e. lower than the threshold creep temperature so that this means that the outer material of the model will

Table 1
Various parameters and results comparison obtained as output from the KIT CFA tool and from the manual calculation for the critical SCL path.

RCC-MRx parameter	Manual calculation	KIT CFA tool output	% Difference
General parameters			
S_m (allowable stress)	167MPa	168.95MPa	-1.2
$3S_m$ rule	324.76MPa	325.5MPa	-0.2
Inner radius total equivalent stress	324.76	324.4MPa	0.1
Outer radius total equivalent stress	212.94	217.7MPa	-2.2
RCC-MRx parameter	Manual calculation	KIT CFA tool output	% Difference
Progressive deformation parameters			
Mean temperature across SCL	425°C	416.86 °C	1.9
SR_1	35.23	14.51	58.8
SR_2	18.53	12.95	30.1
SR_3	19.93	13.25	33.5
v_1	0.0754	0.262	-247
v_2	0.1208	0.278	-15.7
v_3	0.1137	0.263	-131
P_1	127.70MPa	82.06MPa	35.7
P_2	151.61MPa	86.83MPa	42.7
P_3	149.78MPa	85.87MPa	42.7
ε_{p+f} *at* $1.25P_1$	Not applicable	0.546 × 10-3	
ε_{p+f} *at* $1.25P_3$	Not applicable	0.573 × 10-3	
Creep – Fatigue parameters			
RCC-MRx parameter	Manual calculation	KIT CFA tool output	% Difference
Creep – Fatigue parameters			
$\overline{\Delta\varepsilon_{el+pl}}$	0.1486 %	0.1480 %	0.4 %
σ_k	168.19 MPa	167.86MPa	0.2%
σ_k(after stress relaxation)	Not applicable	161.57MPa	
$\overline{\Delta\varepsilon_f}$ per cycle (hold time 1 h)	0.01156 % (relaxation not taken into account)	0.01 % (relaxation taken into account)	13.5%
$\overline{\Delta\varepsilon}$	0.16 %	0.159 %	0.63%
Number of cycles to failure	75504	119671 (relaxation taken into account)	-58%
$V_{inner\ radius}$	0.086	0.11	-27.9%
$W_{inner\ radius}$	0.799	0.74	7.4%

not creep. Nonetheless the authors considered that creep is significant since the inner wall is at 500°C and the average temperature across the wall is 425°C, that is higher than the creep threshold temperature. The second part of the first test cannot be used since the negligible creep curve in A3.31 is not yet available for EUROFER97 steel.

6.2. Type P damage checks

In [15] the negligible irradiation and significant creep type P damage rules are given in RB3252. Before satisfying the latter rules, the rules given in RB3251 must first be satisfied. Using A3.43 and linear interpolation the allowable stress S_m is determined to be equal to 167MPa at the mean wall temperature of 425°C across the SCL used to calculate the primary membrane stress $\overline{P_m}$. Table 1 shows a percentage difference of 1.2% from the S_m value calculated by the KIT CFA rule. This is due to the different way of how the mean temperature was calculated between the two methods resulting in a 1.9% difference in the mean temperature across the cylinder wall so affecting the value of S_m.

Table 2a shows the maximum membrane, bending, membrane + bending and total stresses at the inner and outer radii respectively for the primary stresses. These were determined using the ANSYS Mechanical [33] linearization equations and procedures which are as those

Table 2
(a): Membrane, bending, membrane + bending and total stresses at the inner and outer radii respectively for the primary stress field. (b): Parameters used for the ratchetting check.

(a)	Membrane (MPa)	Bending (MPa)	Membrane+Bending (MPa)	Total (MPa)
Stress intensity				
Inner radius	9.63	6.15	15.62	18.32
Outer radius	9.63	6.15	4.14	5.45
Radial stress				
Inner radius	-2.69	-3.65	-6.34	-7.97
Outer radius	-2.69	3.65	0.96	0
Hoop stress				
Inner radius	8	3.45	11.45	12.96
Outer radius	8	-3.45	4.55	5.46
(b)				
Max θ_m	Max $\overline{P_m}$	Max $\overline{P_L + P_b}$	Max $\overline{\Delta Q}$	
425°C	9.63MPa	18.32MPa	339.36MPa	

required by RCC-MRx [15]. The primary stress field was calculated by applying the internal pressure of 8MPa and using temperature dependant material properties. The linearised longitudinal stresses along the length of the cylinder and the shear stresses are not shown because these are practically zero given the boundary conditions used and the nature of the axisymmetric problem. RCC MRx considers the stress intensity to be the von Mises equivalent stress.

RB3251 requires that the general primary membrane stress intensity

$$\overline{P_m} \leq S_m \tag{1}$$

that the local primary membrane stress intensity

$$\overline{P_L} \leq 1.5S_m \tag{2}$$

and that the local primary membrane plus bending stress intensity

$$\overline{P_L + P_b} \leq 1.5S_m \tag{3}$$

From Table 2a, $\overline{P_m} = 9.63$MPa so that Eq. (1) is satisfied. In this example there are no stress concentrations due to geometry so that $\overline{P_L}$ is equal to $\overline{P_m}$ implying that Eq. (2) is satisfied as well.

From Table 2a, considering the maximum value at the inner radius, $\overline{P_L + P_b} = 15.62$MPa is well below the value of $1.5S_m$ so that Eq. (3) is also satisfied. Since there are no geometric stress concentration points on the SCL it is best to use the value of total stress 18.32MPa for $\overline{P_L + P_b}$ and compare this with $1.5S_m$. Even so Eq. (3) is satisfied.

Considering the rules for significant creep in RB3252, RCC-MRx [15] requires that the creep usage fraction $U(\Omega\overline{P_m}) \leq 1$.

In this example all membrane stresses are classified under general membrane stress so that $\Omega = 1$. To determine the creep usage fraction $U(9.63)$ for $\overline{P_m} = 9.63$MPa the allowable time T_j to prevent excessive creep deformation under the primary membrane stress is found using the S_t curve in A3.52 [15]. For this case the curve for 425°C is extrapolated by a straight line passing through the last two points in a time stress log-log diagram. For $S_t = 9.63$MPa, T_j is determined to be equal to 3.39×10^{34} h. This actually is a very long time and is due to the low value of the general primary membrane stress.

RCC-MRx [15] also requires that the creep usage fraction associated with the sum of the local primary membrane and primary bending

stresses multiplied by the factor $\phi = 0.88$ for a circular cross section tube, $U(\overline{P_L + \phi P_b}) \leq 1$ or $U(\overline{P_m + \phi P_b}) \leq 1$ be satisfied. This check requires that the quantity $\overline{P_m + \phi P_b}$ is determined for the radial and hoop directions as given in Table 2a. The von Mises stress intensity is then calculated using the resulting values for the radial and hoop directions, the value in the longitudinal direction being taken as zero. For the axisymmetric problem the radial, hoop and longitudinal stresses are the principal stresses. The highest membrane plus bending stress intensity occurs at the inner radius so that the check is done at this radius. In the absence of geometric stress concentrations again considering the total stresses gives

$\overline{P_m + \phi P_b} = 17.03MPa$ and again using the S_t curve in A3.52 [15] and the same log-log extrapolation procedure as for $U(\Omega\overline{P_m})$, T_j is determined to be equal to 4.07×10^{28} h.

The long times calculated for excessive creep to occur implies that creep due to the primary membrane and primary membrane plus bending stress intensities will not occur during the lifetime of the component.

6.3. Type S damage checks

6.3.1. Progressive deformation

RCC-MRx requires that ratchetting does not occur in order to be able to use the rules to prevent fatigue damage. The significant creep and negligible irradiation check (RB 3262.111) can be carried out if the rules given in RB 3261.111 for negligible creep are satisfied.

6.3.2. Progressive deformation negligible creep and negligible irradiation

RB 3262.111 in RCC-MRx allows the analyst to use either the method of effective primary stress intensity or the alternative simpler $3S_m$ criterion. The former method compares the effective primary stress intensity with the allowable stress S_m. In this paper both methods are used. Table 2b gives the required parameter values obtained from the FE analysis. $\overline{\Delta Q}$ is obtained from the FE analysis with only the thermal load being applied. Fig. 6a shows that its maximum value occurs at the inner radius.

Using RB3261.1112 for the case without overload of short duration

$$Max(\sigma_m) = Max(\overline{P_m}) = 9.63\text{MPa}$$

$$Max(\sigma_L + \sigma_b) = Max(\overline{P_L + P_b}) = 18.32\text{MPa}$$

$$\Delta q = \overline{\Delta Q} = 339.36\text{MPa}$$

Fig. 6b shows that $Max(\overline{P_L + P_b}) + \overline{\Delta Q} = 324.76$MPa. This is obtained by applying both the pressure load and the thermal load in the FE analysis. Once again since there are no geometric stress concentrations along the SCL the total stress intensity value rather than the membrane plus bending is used in the analyses.

The above shows that the $3S_m$ criterion is satisfied ($3S_m$=501MPa) so that this alternative rule excludes ratcheting.

The method of effective primary stress intensity requires the calculation of a number of parameters and these are shown in Table 3 for the thick cylinder model.

The detailed procedures to calculate the value of these parameters are given in RB3261.1114 to RB3261.1116 of RCC-MRx [15]. The efficiency indices v_1 and v_2 are obtained using the efficiency diagram given in A3.18AS.481 for 9% chrome alloy steel still in probationary phase rule [15]. It must be noted that RCC-MRx [15] does not provide the efficiency diagram for EUROFER97 steel. Until such material property is available it was decided [15,34] that the properties Group A3.18AS are to be applied to components made of alloy steel having approximately 9% chromium and 1% molybdenum in normalised - tempered or quenched - tempered conditions. This therefore applies to EUROFER97 which has 9% chromium and 1% tungsten.

The level A criteria for progressive deformation for ratchetting in the absence of significant creep are given in RB 3261.1117 and material properties $k_{dp1} = k_{dp2} = 1.85$ in A3.18AS.481 as

$$P_1 \leq k_{dp1}.S_m \tag{4}$$

$$P_2 \leq K.k_{dp2}.S_m \tag{5}$$

For plates and shells $K = 1.5$ and S_m is determined at the maximum of

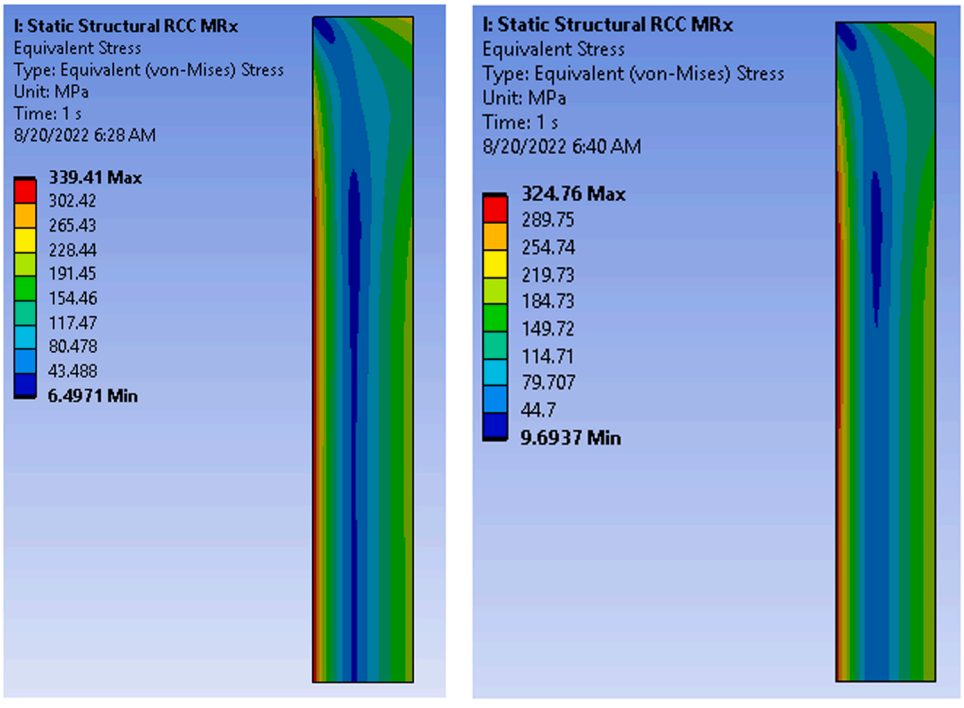

Fig. 6. (a) von Mises stress intensity secondary thermal stress, (b) von Mises stress intensity primary membrane plus bending + secondary thermal stress.

Table 3
Parameters used to calculate the effective primary stress intensities.

$= \frac{\Delta q}{Max(\sigma_m)}$ Secondary ratio in relation to the primary membrane stress	$SR_2 = \frac{\Delta q}{Max(\sigma_L + \sigma_b)}$ Secondary ratio in relation to the sum of primary stresses	For $SR \geq 4$ $\nu_1 = \frac{0.98}{SR_1^{0.72}}$ Efficiency index	For $SR \geq 4$ $\nu_2 = \frac{0.98}{SR_2^{0.72}}$ Efficiency index	$P_1 = \frac{Max(\sigma_m)}{\nu_1}$ Effective primary membrane stress intensity	$P_2 = \frac{Max(\sigma_L + \sigma_b)}{\nu_2}$ Effective primary stress intensity of the sum of primary stresses
35.23	18.53	0.0754	0.1208	127.7MPa	151.61MPa

the mean temperature which occurs across the SCL[15]. Therefore S_m = 167MPa, see Table 1. From the P_1 and P_2 values given in Table 3 and using the values of K and S_m it can be deduced that the criteria given in (4) and (5) are satisfied.

6.3.3. Progressive deformation significant creep and negligible irradiation

RB 3262.112 in RCC-MRx gives the rules to check that progressive deformation under significant creep and negligible irradiation does not occur. The rules are only valid for regions with no geometric stress concentrations so that the rules are valid for the thick cylinder example.

For the thick cylinder example the holding time of the pressure and temperature cycle is one hour. The analysis requires the values of parameters Max θ_m, Max $\overline{P_m}$, Max $\overline{\Delta Q}$ which are given in Table 2b. Section 6.2 gives the value for parameter $\overline{P_L + \phi P_b}$.

There are no secondary membrane stresses in the thick cylinder example so that use is made of RB3262.1112 for the case without overload of short duration. An example for secondary membrane stresses is given by RCC-MRx as that of a cylinder subjected to axial thermal gradients which is not the case for this example.

$$Max(\sigma_m) = Max(\overline{P_m}) \;=\; 9.63\text{MPa}$$

$$Max(\sigma_L + \phi\sigma_b) = Max(\overline{P_L + \phi P_b}) \;=\; 17.03\text{MPa}$$

$$\Delta q = \overline{\Delta Q} = \; 339.36\text{MPa}$$

Using the rules in RB3262.1114 to RB3262.1116 the parameters shown in Table 4 are calculated.

From RB 3262.1117 the strain allowables are given by

$$\varepsilon_{p+f} \; at \; 1.25P_1 \leq D_{max} \tag{6}$$

$$\varepsilon_{p+f} \; at \; 1.25P_3 \leq 2D_{max} \tag{7}$$

where ε_{p+f} in Eq. (6) is the plastic strain plus associated creep strain at 1.25 times the effective primary membrane stress intensity P_1 and where ε_{p+f} in Eq. (7) is the plastic strain plus associated creep strain at 1.25 times the effective primary membrane stress intensity of the sum of primary stresses corrected for the effect of creep P_3.

D_{max} is obtained from A3.56 but since this is not yet available for EUROFER97 [15] the value of 1% strain for A3.18AS.481 9% chrome alloy steel is used. So that the limits on the ε_{p+cr} strain values become

$$\varepsilon_{p+f} \; at \; 1.25P_1 \leq 1\% \tag{8}$$

$$\varepsilon_{p+f} \; at \; 1.25P_3 \leq 2\% \tag{9}$$

The plastic deformation ε_p is determined using A3.45 using the 'average' tensile stress strain curve. The total creep strain ε_f is determined as indicated in A3.54 of RCC-MRx [15].

Therefore from A3.45 for EUROFER97

$$\varepsilon_p = \left[\frac{\sigma}{C_o \times \left(R_{p0.2}\right)_{ave}}\right]^{\frac{1}{n_o}}$$

where ε_p is the plastic strain due to stress σ in MPa

The parameters C_o = 1.085 and n_o = 0.0523 are obtained by linear interpolation and from A3.41 for EUROFER97, $(R_{p0.2})_{ave}$ at 425°C is equal to 425.86MPa so that

ε_p for $1.25P_1 = 1.66 \times 10^{-9}$ % which is a very low value. This was expected since stresses in the thick cylinder are low and

ε_p for $1.25P_3 = 3.151 \times 10^{-8}$ % which is again a very low value.

The primary creep strain can be determined from A3.54 for EUROFER97. The average primary creep strain is calculated using $\varepsilon_f = C_1 t^{c_2} . \sigma^{n_1}$ which is valid for a temperature between 375°C and 600°C. Table A3.19AS.541 of RCC-MRx [15] is used to determine C_1, C_2 and n_1. These parameters are functions of temperature. Since the effective stress intensities P_1 and P_3 were calculated at the maximum value of the mean temperature within the thickness, in this case 425°C, then values of C_1, C_2 and n_1 were determined at this temperature. The minimum temperature for which these parameter values are available in Table A3.19AS.541 is 450°C so that to be conservative the values of C_1, C_2 and n_1 used are those at 450°C so that

$$\varepsilon_f = 3 \; \times 10^{-48} t^{0.49625} . \sigma^{18.538}$$

The average end of primary creep time is given by $t_{fp} = C_3 \sigma^{n_3}$ where σ is in MPa and t is in hours.

At 450°C, $C_3 = 2.09 \times 10^{24}$ and n_3 = -8.29777 so that

$$t_{fp} = 2.09 \; \times 10^{24} . \sigma^{-8.29777}$$

For $1.25P_1$ $t_{fp} = 1.046 \; \times 10^6$ h and

For $1.25P_3$ $t_{fp} = 291.5 \; \times 10^3$ h

The latter is equal to 33 years which is a long time so it was not deemed necessary to calculate secondary creep. Therefore

For $1.25P_1$ and after $t_{fp} = 1.046 \; \times 10^6$ h ε_f=2.24×10^{-4} %

For $1.25P_3$ and after $t_{fp} = 291.5 \; \times 10^3$ h ε_f=2.06×10^{-3} %

Therefore

$$\varepsilon_{p+f} \; at \; 1.25P_1 = 2.24 \; \times 10^{-4} \; \%$$

$$\varepsilon_{p+f} \; at \; 1.25P_3 = 2.06 \; \times 10^{-3} \; \%$$

Therefore the strain allowables given in (8) and (9) are satisfied and the thick cylinder will not fail due to progressive deformation.

Table 1 shows quite large percentage differences between the manually calculated values and the KIT CFA tool values for parameters

Table 4
Parameters used to calculate the effective primary stress intensities.

$= \frac{\Delta q}{Max(\sigma_m)}$ Secondary ratio in relation to the primary membrane stress	$SR_3 = \frac{\Delta q}{Max(\sigma_L + \phi\sigma_b)}$ Secondary ratio in relation to the sum of primary stresses	For $SR \geq 4$ $\nu_1 = \frac{0.98}{SR_1^{0.72}}$ Efficiency index	For $SR \geq 4$ $\nu_3 = \frac{0.98}{SR_3^{0.72}}$ Efficiency index	$P_1 = \frac{Max(\sigma_m)}{\nu_1}$ Effective primary membrane stress intensity	$P_3 = \frac{Max(\sigma_L + \phi\sigma_b)}{\nu_2}$ Effective primary stress intensity of the sum of primary stresses
35.23	19.93	0.075	0.1137	128.4MPa	149.78MPa

SR_1, SR_2, v_1, v_2, v_3, P_1, P_2 and P_3. One of the reasons for these large differences is due to considering the secondary membrane stress Q_m as is done in the KIT CFA tool or not considering these as was done in the manual calculation. The other reason for the large differences is due to either considering the total value of $\overline{\Delta Q}$ due to the thermal stress in the progressive deformation calculations or else considering only the bending part (secondary stress range) of $\overline{\Delta Q}$ over the linearised stress path. Both issues would require further discussion on code interpretation. Another point subject to code interpretation is whether to use the local temperature at the point at which the sum of plastic and creep strain is being calculated to get the material property parameters for the plastic and creep strain equations or else to use the mean temperature through the wall at the SCL under investigation. In this example when the local temperature was used for the material property parameter the sum of plastic and creep strain exceeded the allowables given in Eqs. (8) and (9).

6.3.4. Creep – fatigue

For a creep fatigue assessment RCC-MRx requires that the SCL is not located at a geometric discontinuity where a stress concentration exists. In the thick cylinder example there are no such discontinuities so that the creep fatigue rules can be applied. The creep fatigue assessment requires three steps [15]:

1 Calculate the fatigue usage fraction $V(\overline{\Delta\varepsilon})$ (RB 3262.1123)
2 Calculate the creep rupture usage fraction $W(\sigma)$ (RB 3262.1125)
3 Verify the combined effects of creep and fatigue using the creep – fatigue interaction diagram for the material (A3.55)

6.3.5. The fatigue usage fraction $V(\overline{\Delta\varepsilon})$

The fatigue usage fraction V uses the total stress and the total strain variation during a cycle of loading. Mechanical properties must be taken at the local temperature in the region of interest.

The fatigue usage factor is given by

$$V = \frac{n_i}{N_i(\overline{\Delta\varepsilon})}$$

n_i being the number of cycles applied during the lifetime of the component and N_i being the allowed number of cycles for the total strain variation $\overline{\Delta\varepsilon}$ which is equal to $\overline{\Delta\varepsilon_{el+pl}} + \overline{\Delta\varepsilon_f}$.

$\overline{\Delta\varepsilon_f}$ is the creep strain and accounts for the fact that creep or stress relaxation will increase fatigue damage.

For the thick cylinder example the creep – fatigue analysis is carried out at the SCL at the inner and outer radius. From the FE model and stress field shown in Fig. 6b

$$(\Delta\sigma_{tot\ inner}) = 324.76\ MPa\ at\ \theta_{max} = 500^oC$$

$$(\Delta\sigma_{tot\ outer}) = 212.95\ MPa\ at\ \theta_{max} = 350^oC$$

6.3.6. Determining $\overline{\Delta\varepsilon_{el+pl}}$

Following RB3261.1123

$$\overline{\Delta\varepsilon_{el+pl}} = \overline{\Delta\varepsilon_1} + \overline{\Delta\varepsilon_2} + \overline{\Delta\varepsilon_3} + \overline{\Delta\varepsilon_4} \quad (10)$$

These four strain terms are determined using the cyclic curve (A3.46) corresponding to θ_{max} at the point under examination. The cyclic curve gives the stabilised stress variations for a material subjected to a cyclic loading.

6.3.7. Calculating $\overline{\Delta\varepsilon_1}$

$\overline{\Delta\varepsilon_1}$ is the strain range given by elastic analysis and can be calculated using $\Delta\varepsilon_1 = \frac{2}{3}(1+\upsilon)\frac{\overline{\Delta\sigma_{tot}}}{E\ at\ \theta_{max}}$ [15].

Table 5 gives the resulting values for the inner and outer radii for $\overline{\Delta\varepsilon_1}$. Table 5 also gives a comparison with the elastic stresses calculated using FE analysis. The values are similar within 15% of each other. In this paper the values for $\overline{\Delta\varepsilon_1}$ used are those calculated using the given equation [15].

Table 5
Calculated values for $\overline{\Delta\varepsilon_1}$.

	Inner radius	Outer radius
$\Delta\varepsilon_1 = \frac{2}{3}(1+\upsilon)\frac{\overline{\Delta\sigma_{tot}}}{E\ at\ \theta_{max}}$	0.1481%	0.0927 %
FE analysis	0.17 %	0.107 %
% difference	-14.7 %	-15.4 %

6.3.8. Calculating $\overline{\Delta\varepsilon_2}$

$\overline{\Delta\varepsilon_2}$ is the 'plastic' increase in strain due to the primary stress range at the point under examination and equal to $\Delta[\overline{P_m + 0.67(P_b + P_L - P_m)}]$. For the example being considered $P_L = P_m$ since there is no geometrical discontinuity so that the previous term reduces to $\Delta[\overline{P_m + 0.67(P_b)}]$. FE total stresses are used for the same reason and the stress components are used to calculate the primary stress range from which the von Mises stress intensity is then computed. The following results are obtained

$\Delta[\overline{P_m + 0.67(P_b)}]$ inner radius = 15.42MPa at $\theta_{max} = 500°$C and
$\Delta[\overline{P_m + 0.67(P_b)}]$ outer radius = 6.79MPa at $\theta_{max} = 350°$C

From the cyclic curve A3.46 for EUROFER97 steel the values for $\overline{\Delta\varepsilon_2}$ that are calculated are shown in Table 6. The resulting vales are very small compared with $\overline{\Delta\varepsilon_1}$ and can practically be ignored.

6.3.9. Calculating $\overline{\Delta\varepsilon_3}$

$\overline{\Delta\varepsilon_3}$ represents the 'plastic' increase in strains along path 'c-d' shown in Fig. 7 which is adapted from [15]. For this example, point 'c' in Fig. 7 is given by $(\Delta\sigma_{tot}),\ (\overline{\Delta\varepsilon_1} + \overline{\Delta\varepsilon_2})$ and this point is used to construct Neuber's hyperbola $\overline{\Delta\sigma}.\overline{\Delta\varepsilon} = constant$. Point 'd' is obtained from the intersection of the Neuber's hyperbola with the cyclic curve. Fig. 7 is constructed for both the inner and outer radii at the SCL and these result in the values of $\overline{\Delta\varepsilon_3}$ shown in Table 6.

6.3.10. Calculating $\overline{\Delta\varepsilon_4}$

$\overline{\Delta\varepsilon_4}$ is the 'plastic' increase in strain due to triaxiality and is given by $\overline{\Delta\varepsilon_4} = (K_v - 1)\overline{\Delta\varepsilon_1}$.

The parameter K_v at $\Delta\sigma_{tot}$ values at the inner and outer radii of the thick cylinder is obtained using interpolation from the values given in Table A3.19AS.463 for EUROFER97 steel [15]. Table 6 gives the resulting values for $\overline{\Delta\varepsilon_4}$ and also the values for $\overline{\Delta\varepsilon_{el+pl}}$ using Eq. (10).

$\overline{\Delta\sigma^*}$ is then determined from the cyclic curve (A3.46) for EUROFER97 steel [15] for which the abscissa is equal to $\overline{\Delta\varepsilon_{el+pl}}$. Table 6 gives the values for $\overline{\Delta\sigma^*}$ for the inner and outer thick cylinder radii.

Tables 1 and 6 show a good correlation between the manually calculated value and the KIT CFA tool value for $\overline{\Delta\varepsilon_{el+pl}}$.

6.3.11. Determining $\overline{\Delta\varepsilon_f}$ - the strain amplification due to creep

For EUROFER97 steel, creep strain occurs in the regions where the temperature θ^*during the holding time is higher than 375°C. For the

Table 6
Calculated values for $\overline{\Delta\varepsilon_2}$, $\overline{\Delta\varepsilon_3}$, $\overline{\Delta\varepsilon_4}$, $\overline{\Delta\varepsilon_{el+pl}}$, $\overline{\Delta\sigma^*}$.

	Inner radius	Outer radius
$\overline{\Delta\varepsilon_2} = (\frac{\overline{\Delta\sigma}}{K})^{\frac{1}{m}}$	1.07×10^{-21} %	4.87×10^{-18} %
$\overline{\Delta\varepsilon_3}$	1×10^{-4} %	5×10^{-6} %
$\overline{\Delta\varepsilon_4}$	0.000368 %	0 %
$\overline{\Delta\varepsilon_{el+pl}}$	0.1486 %	0.0928%
$\overline{\Delta\sigma^*}$	325.24 MPa	212.93 MPa

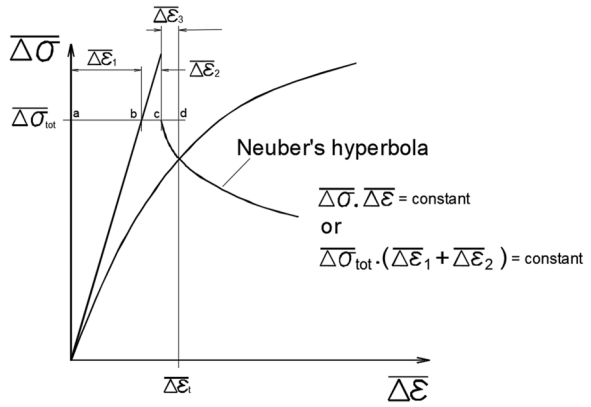

Fig. 7. Graphical description of how to determine $\overline{\Delta\varepsilon_3}$using the cyclic curve for EUROFER97 (adapted from [15]).

thick cylinder example such a region occurs at the inner radius so that $\overline{\Delta\varepsilon_f}$ is determined at this radius. The strain amplification due to creep per cycle is obtained by using the creep rule for the material at a stress σ_k. To calculate σ_k, RCC-MRx requires the parameters shown in Table 7 to be determined.

$\overline{\Delta\sigma^*}$ for the inner radius is obtained from Table 6. The equation giving the value of $\overline{P}_{max}$ is used at the stress component level using the latter stress values given in Table 2a. The primary stress range $\overline{\Delta P}$ is obtained from the calculation of $\overline{\Delta\varepsilon_2}$. The secondary stress range $\Delta S^* = \overline{\Delta\sigma^*} - \overline{\Delta P}$ is obtained by scalar addition [15]. The symmetrisation coefficient K_s is obtained using the ratio $\frac{\overline{\Delta\sigma^*}}{2(R_{p0.2})_{min}}$ and Fig. A3.19AS.464 in A3.46 for EUROFER97 steel [15]. The value of K_s is out of range in the latter figure and therefore a value of 0.5 is used.

For this example the value of σ_k is calculated using Fig. RB3262.1123b and the reduced cyclic curve which is obtained by dividing by two the coordinates of the cyclic curve given in (A3.46) [15]. σ_k is obtained as the ordinate of the curve corresponding to the sum of the strains ε_p and ε_s corresponding to $\overline{P}_{max}$ and $K_s\overline{\Delta S^*}$ respectively. The resulting value of σ_k and the corresponding creep strain per cycle $\overline{\Delta\varepsilon_f}$ (hold time 1 h) calculated using the creep strain equations for EUROFER97 [33] are given in Table 7. The analysis shows that the end of the primary creep phase is 4.8×10^6 h which is a very long time so that it is hypothesised that creep will remain in the primary phase.

Tables 1 and 7 show a good correlation between the manually calculated value and the KIT CFA tool value for σ_k. In order to calculate a less conservative value for the creep strain per cycle, RCC-MRx allows the analyst to relax the secondary part of the stress σ_k i.e. $K_s\overline{\Delta S^*}$ throughout the hold time. Relaxation is not taken into account in this paper for the manual calculation and this explains the difference shown for $\overline{\Delta\varepsilon_f}$when compared to the corresponding value obtained from the KIT CFA tool. The latest version of the KIT CFA tool takes stress relaxation into consideration (Table 1).

The total strain variation per cycle $\overline{\Delta\varepsilon}$ used to calculate the fatigue usage fraction is obtained from $\overline{\Delta\varepsilon_{el+pl}} + \overline{\Delta\varepsilon_f}$. Using the respective values from Tables 6 and 7, $\overline{\Delta\varepsilon}$ at the inner radius is given by 0.16% which compares well with the value given in Table 1 calculated using the KIT CFA tool.

The value of $\overline{\Delta\varepsilon} = 0.16\%$ is used in the RCC-MRx section RB 3226.2 together with the fatigue curves for EUROFER97 steel to calculate N, the number of cycles to failure.

The value of N thus obtained is equal to 8.776×10^5 cycles so that the fatigue usage factor per cycle at the inner radius is given by

$$V_{cycle\ inner\ radius} = \frac{1}{8.776 \times 10^5} = 1.139 \times 10^{-6}$$

The material at the outer radius does not creep so that from Table 6 $\overline{\Delta\varepsilon} = \overline{\Delta_{el+pl}} = 0.0928$. This gives a fatigue usage factor of 4.2×10^{-9}.

6.3.12. *The creep rupture usage fraction* W(σ)

For the outer radius of the thick cylinder, the creep rupture usage fraction $W_{cycle\ outer\ radius}$ is zero since the temperature in the region is below the creep temperature for the material.

For the inner radius, use is made of the minimum creep rupture stress curves S_r given in A3.53 for EUROFER97 [15] in which log-log extrapolation is required to calculate the creep rupture time at an S_r value equal to $\frac{\sigma_k}{0.9} = 187.3\ MPa$. This results in the creep rupture time to be equal to 94664 h so that the creep rupture usage fraction at the inner radius is given by $W_{cycle\ inner\ radius} = \frac{1}{94664} = 1.056 \times 10^{-5}$.

6.3.13. *The creep - fatigue interaction diagram*

The fatigue usage fraction $V(\overline{\Delta\varepsilon})$ and the creep rupture usage fraction $W(\sigma)$ are used in conjunction with the creep - fatigue interaction diagram for the EUROFER97 material found in A3.55 [15] in order to determine the cycles to failure at the inner radius region in the presence of creep. The surface at the inner radius dominates fatigue creep failure. Fig. 8 shows a representation of the creep - fatigue interaction diagram for EUROFER97 and was used to locate the RCC MRx limits for creep fatigue failure at the inner radius. At this limit the fatigue and creep damage are calculated to have values of 0.086 and 0.799 respectively.

Dividing the fatigue damage by the fatigue usage fraction per cycle at the inner radius gives a fatigue creep life of 75504 cycles.

The difference in creep fatigue life between that calculated manually and that calculated using the KIT CFA tool is 58%. This is quite a high difference and the main reason is the issue that in the manual calculation relaxation of the secondary stress was not taken into account which results in more creep damage that reduces the fatigue life.

Table 7
Parameters and other values required to determine $\overline{\Delta\varepsilon_f}$at the inner radius.

Parameters or calculated values	Inner radius
$\overline{\Delta\sigma^*}$	325.24 MPa
θ^*	500°C
$\overline{P}_{max} = Max[\overline{P_m + 0.66(P_b + P_L - P_m)}]\ P_L = P_m$	13.57 MPa
The primary stress range $\overline{\Delta P}$	15.42 MPa
The secondary stress range $\Delta S^* = \overline{\Delta\sigma^*} - \overline{\Delta P}$	309.82 MPa
Symmetrisation coefficient K_s	0.5
σ_k	168.19 MPa
$\overline{\Delta\varepsilon_f}$ per cycle (hold time 1 h)	0.011558 %

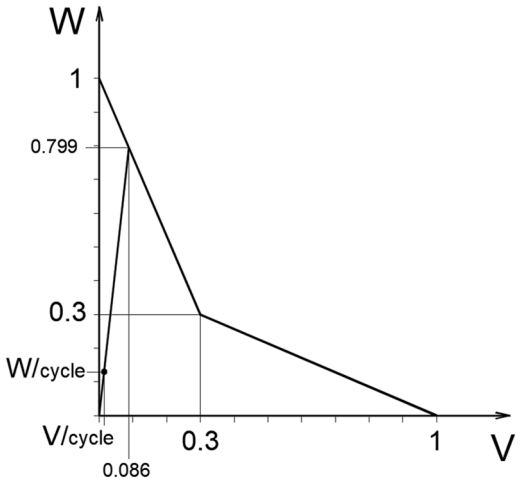

Fig. 8. Creep - Fatigue interaction diagram (EUROFER97) for the inner radius region of the thick cylinder (adapted from [15]).

7. Comparison of results between the manual calculation and the KIT CFA tool

For the thick cylinder model the difference in creep fatigue life between that calculated manually and that calculated using the KIT CFA tool is 58%. Tables 1 and 7 show a good correlation between the manually calculated value and the KIT CFA tool value for the initial value for σ_k that is the stress used to calculate the creep strain. Table 1 also shows a good correlation between the manually calculated value and the KIT CFA tool values for $\overline{\Delta\varepsilon_{el+pl}}$ and $\overline{\Delta\varepsilon}$ at the inner radius. These are used to determine the fatigue usage fraction $V(\overline{\Delta\varepsilon})$. In order to calculate a less conservative value for the creep strain per cycle and also the creep rupture usage fraction, RCC-MRx allows relaxation of the secondary part of the stress σ_k throughout the hold time. Unlike in the KIT CFA tool, relaxation is not taken into account in this paper for the manual calculation and this explains the difference shown for $\overline{\Delta\varepsilon_f}$when compared to the corresponding value obtained from the KIT CFA tool. The difference in creep strain affects the fatigue creep life so that stress relaxation is partly the reason for the large difference in creep fatigue life between that calculated manually and that calculated using the KIT CFA tool. The same analysis was carried out using the KIT tool without considering stress relaxation to calculate the creep strain. The creep fatigue life as given by the KIT CFA tool was then calculated to be 81,508 cycles. This differs from the one obtained from the manual calculation by 8% indicating that when stress relaxation is not taken into account the calculated creep fatigue life would then be highly conservative.

It has also been noticed that the fatigue life is very sensitive to small changes in total strain variation values. This implies that for consistent results the total strain needs to be calculated as accurately as possible with a high amount of repeatability between different analysts.

Furthermore Table 1 shows quite high percentage differences between the manually calculated values and the KIT CFA tool parameter values used for the progressive deformation check which would require further discussions on code interpretation.

Another point subject to code interpretation for the progressive deformation check for significant creep is whether to use the local temperature at the point at which the sum of plastic and creep strain is being calculated to get the material property parameters for the plastic and creep strain equations or else to use the mean temperature through the wall at the SCL under investigation.

8. Application cases for the DEMO divertor

The motivation behind the work presented in this paper is to review the creep fatigue rules of RCC-MRx and their interpretation and implementation in the KIT CFA tool. This has been done for a simple thick cylinder model with the intend of applying the tool to DEMO divertor components. Previous literature indicated that the inboard reflector plates of the single null divertor dual circuit model have a temperature which is above the creep threshold temperature for EUROFER97 steel. These supports can be potential applications for a creep fatigue assessment. Having said that the same supports are not be meeting the P-type check allowables because of the reduced mechanical properties at high temperatures. This would require a re-design which may then affect the need for a creep fatigue assessment. Even so, a fatigue assessment is always required to determine the fatigue usage fraction and check that it does not go beyond the value of unity during the lifetime of the component.

Previous literature has considered the 1st and 2nd category of operating conditions which include normal operation and normal operating incidents, start up and shutdown emergency conditions. The 3rd category of operating conditions includes emergency conditions having low probability of occurrence but which would require plant shut down and the necessary inspection. The 4th category of operating conditions are highly improbable but may need to be considered because of safety reasons. An example of such emergency loading is that which may occur if cooling water pressure is lost causing the temperature of divertor components to rise above the material creep temperatures. Structural integrity assessment would require the determination of plastic and creep strains for an eventual excessive deformation, plastic instability and low cycle fatigue check. Material softening due to thermal aging and embrittlement brought about by high thermal stress, low temperatures and irradiation would also need to be taken into consideration.

9. Conclusion

The work presented in this paper gives a brief description of the DEMO divertor, its development and an overview of the type of loadings that it will experience during operation. Important structural analyses include those of excessive deformation, creep rupture, progressive deformation, fatigue and creep. The creep fatigue assessment is of particular interest for some of the DEMO divertor components because of the temperatures reached during service which would be above the creep temperatures of the material concerned.

A thick cylinder benchmark example has been developed following the RCC-MRx type P and type S design checks. The example uses similar type of loading as seen by DEMO divertor components. Manual calculations have been performed and compared with the available KIT CFA tool results for the same example. Some results show good correlation between the analyses but others do not. The analysis therefore serves to highlight the importance of proper and consistent code rules' interpretation and the importance of using updated material properties. The database for EUROFER97 material properties is still being updated and when properties were not yet available, values from a similar steel had to be used.

The resulting differences between the manual calculations and the KIT CFA tool give scope for further collaboration between research groups on updated material properties and code interpretation issues. Code creep fatigue assessments require lengthy calculations which tend to become quite complicated. This indicates that a tool such as the one being developed by KIT is very important for performing creep fatigue assessments of divertor and other in vessel components.

The work leads towards necessary creep fatigue assessments of DEMO divertor components that are currently in the development process and also to feedback on the KIT CFA tool as an aid to finetune it for DEMO divertor components.

CRediT authorship contribution statement

M. Muscat: Methodology, Investigation, Writing – original draft, Writing – review & editing. **P. Mollicone:** Methodology, Investigation, Writing – review & editing. **J.H. You:** Conceptualization, Methodology, Funding acquisition, Writing – review & editing. **N. Mantel:** Conceptualization, Methodology, Funding acquisition, Writing – review & editing. **M. Jetter:** Investigation, Writing – review & editing.

Declaration of Competing Interest

The authors declare that they have no known competing financial interests or personal relationships that could have appeared to influence the work reported in this paper.

Data availability

No data was used for the research described in the article.

Acknowledgment

This work has been carried out within the framework of the

EUROfusion Consortium, funded by the European Union via the Euratom Research and Training Programme (Grant Agreement No 101052200 — EUROfusion). Views and opinions expressed are however those of the author(s) only and do not necessarily reflect those of the European Union or the European Commission. Neither the European Union nor the European Commission can be held responsible for them.

References

[1] J.H. You, Divertor of the European DEMO: Engineering and technologies for power exhaust, Fusion Eng. Des. 175 (2022), 113010.
[2] J.H. You, et al., Conceptual design studies for the European DEMO divertor: Rationale and first results, Fusion Eng. Des. 109–111 (Part B) (2016) 1598–1603.
[3] J.H. You, et al., Progress in the initial design activities for the European DEMO divertor: subproject "Cassette, Fusion Eng. Des. 124 (2017) 364–370.
[4] U. Bonovolonta, EU-DEMO divertor: Cassette design and PFCs integration at pre-conceptual stage, Fusion Eng. Des. 159 (2020), 111784.
[5] G. Mazzone, Eurofusion-DEMO divertor – Cassette design and integration, Fusion Eng. Des. 157 (2020), 111656.
[6] J.H. You, Nuclear loads and nuclear shielding performance of EU DEMO divertor: A comparative neutronics evaluation of two interim design options, Nucl. Mater. Energy 23 (2020), 100745.
[7] J.H. You, M. Li, K. Zhang, Structural lifetime assessment for the DEMO divertor targets: Design-by-analysis approach and outstanding issues, Fusion Eng. Des. 164 (2021), 112203.
[8] P. Frosi, G. Mazzone, J.H. You, Structural design of DEMO Divertor Cassette Body: provisional FEM analysis and introductive application of RCC-MRx design rules, Fusion Eng. Des. 109-111 (2016) 47–51.
[9] Design and construction rules for mechanical components of nuclear installations: high temperature, Research and Fusion Reactors, RCC-MRx, AFCEN, 2012. Edition.
[10] P. Frosi, Structural analysis of DEMO divertor cassette body and design study based on RCC-MRx, Fusion Eng. Des. 124 (2017) 628–632.
[11] P. Frosi, Further improvements in the structural analysis of DEMO Divertor Cassette body and design assessment according to RCC-MRx, Fusion Eng. Des. 138 (2019) 119–124.
[12] D. Marzullo, Progress in the pre-conceptual CAD engineering of European DEMO divertor cassette, Fusion Eng. Des. 146 (2019) 942–945.
[13] Marzullo D., EUROfusion report 2NSLJP: Divertor system detailed design description (2020).
[14] Frosi P., EUROfusion report 2P8PER: Loads specifications and structural analysis, (2020).
[15] Design and construction rules for mechanical components of nuclear installations: high temperature, Research and Fusion Reactors, RCC-MRx, AFCEN, 2018. Edition.
[16] Frosi P., EUROfusion report EFDA_D_ 2P7ZLA: Loads Specification (LS) for Divertor Assembly 2020 (incl. neutronic analysis and structural integrity report), (2021).
[17] Y. Lejeail, Application case of RCC-MRx 2012 code in significant creep, in: Proceedings of the ASME Pressure Vessels & Piping Conference, PVP2014, Anaheim, California, USA, 2014. July 20-24.
[18] T. Lebarbe, Consideration of creep in design rules of AFCEN RCC-MRx 2012 code, in: Proceedings of the ASME Pressure Vessels & Piping Conference, PVP2013, Paris, France, 2013. July 14-18.
[19] P. Lamagnere, Design rules for ratchetting damage in AFCEN RCC-MRx 2012 code, in: Proceedings of the ASME Pressure Vessels & Piping Conference, PVP2014, Anaheim, California, USA, 2014. July 20-24.
[20] A. Martin, Efficiency diagram alternative rule for ratchetting: historical background, overview, on-going developments, in: Proceedings of the ASME Pressure Vessels & Piping Conference, PVP2018, Prague, Czech Republic, 2018. July 15-20.
[21] T. Lebarbe, RCC-MRx edition 2015: Overview of three years of developments, in: Proceedings of the ASME Pressure Vessels & Piping Conference, PVP2015, Boston, Massachusetts, USA, 2015. July 19-23.
[22] H.Y. Lee, Development of a program for high-temperature design evaluation according to RCC-MRx, Nucl. Eng. Des. 324 (2017) 181–195.
[23] F. Ozkan, J. Aktaa, Creep fatigue assessment for EUROFER components, Fusion Eng. Des. 100 (2015) 536–540.
[24] Aktaa J., EUROfusion report 2NFUTP: Report on Creep-Fatigue interaction tool development and updates on high temperature effects on DDC (2017).
[25] M. Mahler, F. Özkan, J. Aktaa, ANSYS Creep-Fatigue Assessment tool for EUROFER97 components, Nuclear Materials and Energy 9 (2016) 535–538.
[26] M. Mahler, J. Aktaa, Eurofer97 creep-fatigue assessment tool for ANSYS APDL and workbench, Nucl. Mater. Energy 15 (2018) 85–91.
[27] J. Aktaa, et al., Creep-fatigue design rules for cyclic softening steels, Int. J. Fatigue 118 (2019) 98–103.
[28] ASME, Boiler Presssure & Vessel Code, Section III, Division 1, Subsection NH, Appendix T, ASME, 2004.
[29] Jetter M., EUROfusion report EDFA_D_2NNHWF: Development of assessment tools for creep fatigue interaction and brittle fracture rules (2018).
[30] Jetter M., EUROfusion report 2PHAKD: Creep-Fatigue Assessment Tool (2020).
[31] Jetter M., Aktaa J., EUROfusion report EFDA_D_2PDBVJ: Creep fatigue assessment tool (2021).
[32] Raphael D. M., EUROfusion report EFDA_D_2PCVQQ: Application of DDC-IC rules to breeder blanket component - CEA 2021.
[33] ANSYS WorkBench, ANSYS Mechanical, Academic research license, release 2022R1, 2023.
[34] M. Jetter, Private Communication, Karlsruhe Institute of Technology, KIT, 2022.